Original Research

Hybrid ZnS-MoS_2 Anti-Reflection Additive Nano-coatings for Superior Light Trapping and Power Conversion in Silicon Solar Cells

Naser A. Alsaleh*

Industrial Engineering Department, College of Engineering, Imam Mohammad Ibn Saud Islamic University (IMSIU), Riyadh 11432, Saudi Arabia

Correspondence: naalsaleh@imamu.edu.sa

Received: June 7, 2026; Accepted: August 19, 2026

Abstract: This study investigates the optical and photovoltaic performance of Zinc sulphide (ZnS), molybdenum disulfide (MoS_2), and ZnS/MoS_2 composite anti-reflection coatings deposited on monocrystalline silicon solar cells by radio frequency (RF) magnetron sputtering. Bare, ZnS-coated, MoS_2-coated, and ZnS/MoS_2 composite-coated samples were compared using structural, morphological, optical, electrical, photovoltaic, and thermal analyses. The ZnS/MoS_2 composite coating showed the best performance, reducing reflectance to 5.56% and increasing transmittance to 94.15%. The coated cell achieved a short-circuit current density of 42.37 mA/cm^2, an open-circuit voltage of 0.648 V, a fill factor of 80%, and a power conversion efficiency of 21.96%. The surface temperature of the composite-coated cell was approximately 33 °C under the tested conditions. These results demonstrate that the ZnS/MoS_2 composite coating can improve light management and photovoltaic performance in monocrystalline silicon solar cells.

Keywords: Monocrystalline Silicon Solar Cells; Anti-Reflection Coating (ARC); Zns/MoS_2 Coating; RF Magnetron Sputtering; Power Conversion Efficiency (PCE)

1. Introduction

Evolving global energy markets and the critical need to curb environmental pollution and climate change have driven a widespread shift toward renewable energy sources. However, non-renewable fuel sources still meet over 75% of the world's energy needs while renewable sources are expected to account for around 20% of global energy use by 2030. There have been huge investments in renewable energy by the governments and research institutions worldwide. Renewable energy sources are expected to generate more electricity than any other energy source by 2030, accounting for about 45% of electricity generated. The global solar photovoltaic capacity is expected to nearly triple over the next five years[1].

Solar energy is one of the most promising renewable energy sources because it is abundant and environmentally friendly[2]. The global solar PV capacity is rising; it went from merely 1.3 GW at the start of the millennium to more than 1500 GW as of 2025 and the current pace of expansion remains consistent, with future increases expected to exceed 30% annually. Crystalline silicon (c-Si) is still the prevalent material used in the photovoltaics (PV) industry, and is responsible for more than 95% of the total global PV modules market[3]. However, one of the major reasons hindering efficiency results in silicon cells is optical losses resulting from the reflection phenomenon[4,5].

The bare silicon cells exhibit a high refractive index (n ≈ 3.4-4.0), leading to over 30%-35% of reflection of incoming solar energy. High reflectivity will prevent most of the photons from entering the semiconductor substrate, thereby reducing the creation of electron-hole pairs and short-circuit current (JSC). Anti-reflection coating (ARC) technology is a significant part of the solar cell manufacturing process to minimise optical losses. It is possible to achieve destructive interference to minimise reflections at the air-silicon boundary by applying a thin layer of dielectric or semiconductor material with appropriate refractive index and thickness[6]. Uzum et al. revealed that advanced anti-reflection coatings are essential for silicon solar cells to mitigate optical losses, as bare silicon reflects over 30% of incident energy due to its high refractive index[7]. Chen demonstrated that while single-layer coatings are effective, they are typically optimized for a narrow bandwidth, leading to significant reflection in the ultraviolet and near-infrared ranges[8]. To address this, Kanmaz et al. proposed that composite thin film stacks utilizing a graded refractive index effect create an "optical staircase" between air and silicon, facilitating broadband light absorption from 300 to 1200 nm[9].

Single layer anti-reflection coatings (SLARCs) include Silicon Nitride (Si_3N_4), Silicon dioxide (SiO_2), Titanium dioxide (TiO_2), Aluminum oxide (Al_2O_3), Magnesium fluoride (MgF_2) and Zinc sulphide (ZnS). Although single-layer anti-reflection coatings are effective, they generally provide minimum reflection only over a limited wavelength range. In other words, significant reflection will occur in the ultraviolet (UV) and near-infrared (NIR) ranges of the electromagnetic spectrum[10]. Double Layer Anti-Reflection Coatings (DLARCs) have been developed to address the issue of narrow bandwidth in the optimization of these materials. A DLARC uses the concept of graded refractive indices by placing high index materials adjacent to silicon and low index adjacent to air. This graded design enables a stepwise transition for photons, achieving broadband anti-reflection across the 300-1200 nm solar spectrum[11]. Among others, Transition Metal Dichalcogenides (TMDs), specifically molybdenum disulfide (MoS_2), have been identified as very promising candidates for next generation ARCs. This is a 2D material with tuneable bandgap, high mobility and high absorption coefficients[12]. Zinc sulphide (ZnS) has a high refractive index (2.3), good optical transmittance in the visible region and a wide energy bandgap[13].

The overall experimental workflow adopted in this study is summarized in **Figure 1**.

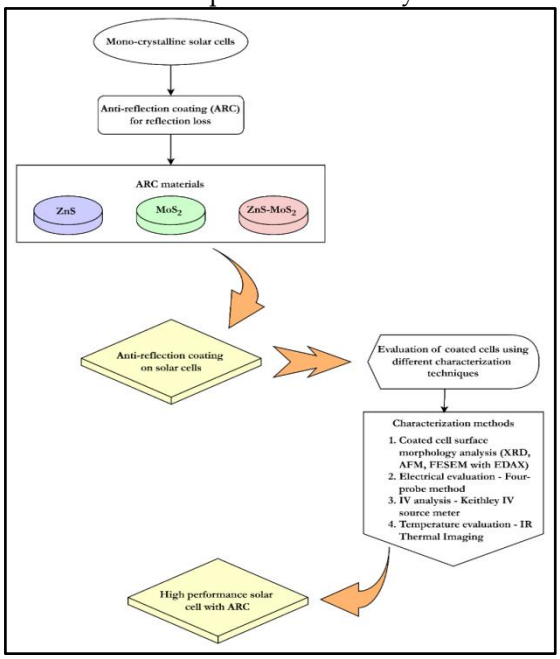


Figure 1. Flowchart of the experimental research process for ZnS/MoS_2 anti-reflection coatings on monocrystalline silicon solar cells

The material selection and the accuracy of the deposition technique are key to an efficient ARC. Although wet chemical methods such as sol-gel and spin coating are relatively easy to implement, they generally do not meet the requirements for high performance DLARCs in terms of the accuracy of the stoichiometry and the uniformity of the thickness. Therefore, radio frequency (RF) magnetron sputtering is mainly used for these coatings. This deposition procedure yields a dense coating with excellent adhesion and nanometer-scale thickness control due to the high kinetic energy of the atoms. However, it is vital to maintain control of the thickness to fulfil the quarter-wavelength requirement[14]. Recent developments in additive manufacturing-based cladding technologies, including laser cladding, wire arc additive manufacturing, and directed energy deposition, have demonstrated that coating composition, process parameters, and microstructural control strongly influence interfacial bonding and functional performance. Recent WAAM-based studies have shown that reinforcement addition and process optimization can improve coating hardness, wear resistance, and structural integrity[15,16]. Although these metallic cladding processes differ from thin-film anti-reflection coatings, they provide useful principles for controlling coating uniformity, composition, interface quality, and performance during advanced surface engineering.

Previous studies have investigated ZnS, MoS_2, and ZnS/MoS_2-based anti-reflection coatings for improving the optical and photovoltaic performance of silicon solar cells[12,17]. However, many reported studies have primarily focused on individual optical or photovoltaic parameters, while a systematic correlation among coating structure, surface morphology, optical response, electrical transport, photovoltaic performance, and operating-temperature behaviour remains insufficiently established. Therefore, the novelty of the present work does not arise solely from the selection of ZnS and MoS_2 as anti-reflection materials. Rather, it lies in the controlled fabrication and comprehensive evaluation of an RF-magnetron-sputtered ZnS/MoS_2 coating on commercial monocrystalline silicon solar cells, together with a direct comparison of bare, ZnS-coated, MoS_2-coated, and ZnS/MoS_2-coated cells prepared and tested under identical conditions. The study combines X-ray diffraction (XRD), atomic force microscopy (AFM), field-emission scanning electron microscopy (FESEM) with energy-dispersive X-ray analysis (EDAX), and ultraviolet-visible-near-infrared (UV-Vis-NIR) spectroscopy, together with Hall-effect measurements, current-voltage characterization, and thermal imaging to establish the relationship between coating structure and the resulting optical, electrical, photovoltaic, and thermal performance. The optimized ZnS/MoS_2 coating produced a minimum reflectance of 5.56%, a maximum transmittance of 94.15%, a power conversion efficiency of 21.96%, and a reduced operating surface temperature of approximately 33°C. Thus, the specific contribution of this work is the integrated experimental demonstration that the sputtered ZnS/MoS_2 coating simultaneously improves broadband light management, charge-transport characteristics, photovoltaic conversion, and thermal behaviour in monocrystalline silicon solar cells.

2. Materials and Methods

2.1. Materials

High-purity ZnS and MoS_2 powders, with a purity exceeding 99.9%, were procured from Chemsol Saudi Arabia. The substrate used for the deposition was commercial-grade monocrystalline silicon (m-Si) solar cells with dimensions of 52 mm x 52 mm, purchased from Solar Arabia Company Ltd, Saudi. To ensure consistency in the deposition process and the structural integrity of the resulting thin films, a pre-processing stage was conducted on the received powders to achieve high uniformity before they were loaded into the deposition system.

2.2. Substrate Preparation

Commercial-grade monocrystalline silicon solar cells were utilized as the base substrate. The monocrystalline cells were selected due to their superior lattice consistency and higher baseline efficiency compared to multi-crystalline alternatives, providing a more precise platform to evaluate

the efficacy of the anti-reflection coatings. Prior to the deposition process, the substrates underwent a rigorous chemical cleaning procedure to remove native oxides, organic contaminants, and dust particles. The cells were ultrasonically cleaned in a sequential bath of acetone, ethanol, and deionized water for 15 minutes each, followed by drying under a high-purity nitrogen stream to ensure a pristine surface for film adhesion.

2.3. RF Sputtering Deposition Method

High-density solid targets were prepared for the RF magnetron sputtering process. In this study, the targets were fabricated using a Universal Testing Machine (UTM) to ensure the precise application of compaction pressure. The ZnS, MoS_2, and blended ZnS/MoS_2 powders were first ground thoroughly to obtain a fine and uniform particle distribution. Then, 10 g of each powder was separately loaded into a precision stainless-steel die and compacted under a uniaxial pressure of 1.5 GPa. The applied pressure produced pellets with a diameter of 50 mm and a thickness of 5 mm. After compaction, the pellets were sintered at 550 °C using a gradual heating and cooling cycle. This treatment improved particle bonding, reduced the possibility of pellet breakage, and provided sufficient mechanical strength for handling and RF magnetron sputtering.

RF magnetron sputtering was employed to deposit ZnS, MoS_2 and ZnS/MoS_2 composite thin films on the prepared monocrystalline silicon solar cells. Four samples were prepared: bare silicon, ZnS-coated silicon, MoS_2-coated silicon, and ZnS/MoS_2 composite-coated silicon. The target-to-substrate distance was maintained at 60 mm, and the coatings were deposited at an RF power of 100 W for 40 min. These parameters were chosen based on preliminary deposition trials and stable plasma operation. Deposition was initiated following 10 minutes of pre-sputtering to remove surface contaminants from the targets and stabilize the plasma. After the chamber reached a base pressure of 2×10^{-6} mbar, high-purity argon gas was introduced at a flow rate of 20 sccm. The working pressure was maintained at 1.0×10^{-2} mbar throughout the deposition. No external substrate heating was applied, and the substrates remained at ambient chamber temperature. Based on the cross-sectional FESEM thicknesses, the average deposition rates were approximately 27.98 nm/min for ZnS, 30.43 nm/min for MoS_2, and 33.23 nm/min for the ZnS/MoS_2 composite coating.

2.4. Characterization Techniques

Physical, structural and morphological features of the coated films have been thoroughly investigated by means of various analytical procedures. The structures of the ZnS and MoS_2 films were studied using XRD to determine their crystal structures and orientations. The surface morphology was examined using AFM to estimate the surface roughness and texture which influenced the process of light scattering. The FESEM-EDAX analysis of the films was performed to confirm the film thickness and composition at high magnification. For optical reflectance and transmittance analyses, ZnS, MoS_2, and ZnS/MoS_2 composite coatings were also deposited on transparent glass substrates under the same sputtering conditions used for the silicon solar cells. The reflectance and transmittance spectra were measured using a UV-Vis-NIR spectrophotometer over the wavelength range of 300-1200 nm, with an uncoated glass substrate used as the reference. The current-voltage (I-V) parameters and PCE were measured outdoors under clear-sky conditions between approximately 11:00 AM and 1:00 PM. Since the incident solar spectrum and cell temperature were not controlled according to standard AM 1.5G conditions, the reported photovoltaic parameters are considered outdoor experimental results rather than standard solar-simulator values.

3. Results and Discussion

3.1. Structural Analysis (XRD)

Figure 2 presents the XRD patterns of bare silicon, ZnS, MoS_2 and composite ZnS/MoS_2 coated

silicon solar cells. X-ray diffraction was performed over the 2θ range from 10° to 80° using the copper Kα radiation (λ = 1.5406 Å). Pure silicon exhibited distinct crystalline peaks at 28.44°, 47.30°, 56.11° and 69.15° which correspond to the (111), (220), (311) and (400) planes of crystalline silicon, respectively, confirming the high crystallinity of the commercially acquired silicon wafer. Similar peak positions have been reported for cubic silicon in other photovoltaic studies. After deposition of the ZnS coating layer, new peaks were observed at 33.02° and 58.88°, corresponding to the (200) and (110) planes of nanocrystalline ZnS. The diffraction peak near 14.33° for the MoS_2 coated silicon substrate was indexed to the (002) crystal plane of MoS_2 layers. The remaining peaks at 39.71° and 44.08° correspond to the diffraction from (103) and (006) planes of MoS_2, respectively, demonstrating that partially crystallized layers of MoS_2 were formed on the silicon substrate. The composite ZnS/MoS_2 coating exhibited the most complex diffraction pattern with overlapping peaks of ZnS and MoS_2 materials.

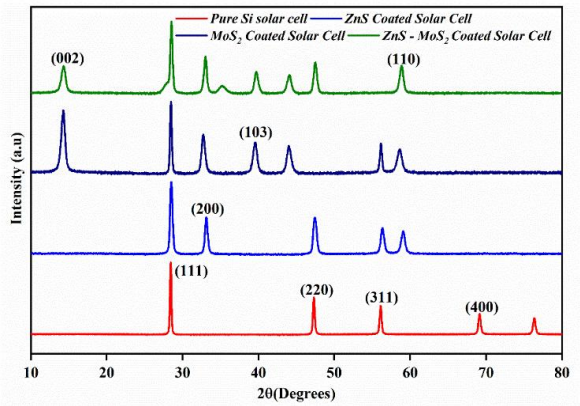


Figure 2. XRD spectra of bare, ZnS, MoS_2, and composite ZnS/MoS_2 coated silicon solar cells

3.2. Surface Topography and Roughness Evaluation (AFM)

The surface topographic features and root-mean-square (RMS) values of the silicon solar cell coatings were analysed using AFM. The two-dimensional (2D) and three-dimensional (3D) AFM images of the coatings are shown in **Figure 3**. The RMS roughness values of the bare, ZnS, MoS_2, and ZnS/MoS_2 coated samples were 90, 108, 116, and 128 nm, respectively. The relationship between RMS surface roughness and reflectance was quantitatively evaluated for the four investigated samples. The RMS roughness values of the bare, ZnS-coated, MoS_2-coated, and ZnS/MoS_2 composite-coated samples were 90, 108, 116, and 128 nm, respectively. Their corresponding reflectance values were 21.95%, 15.78%, 12.03%, and 5.56%. Pearson correlation analysis produced a coefficient of (r = -0.992), indicating a strong inverse correlation between surface roughness and reflectance within the investigated sample set.

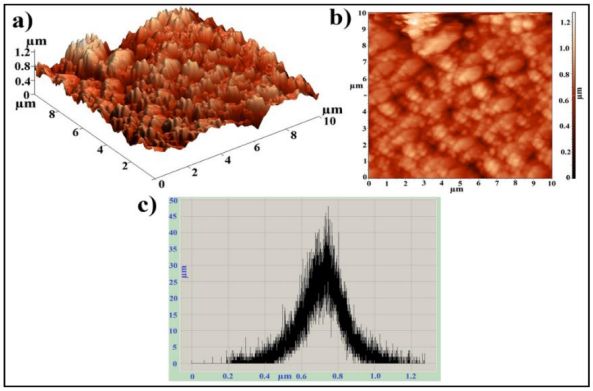


Figure 3. AFM images of the ZnS/MoS_2 coating substrate: (a) 3D surface morphology, (b) 2D surface topography, and (c) Surface roughness histogram illustrating the height distribution of the coated layer

This result suggests that the increased surface texture may contribute to enhanced light scattering and reduced direct reflection. However, reflectance is also influenced by coating composition, thickness, optical constants, and interface quality. Therefore, the present correlation should be interpreted as an experimental trend rather than evidence that surface roughness is the only controlling factor. In summary, the generated surface properties correlate with enhanced light trapping, reduced surface recombination, and ultimately higher JSC and PCE. The increased surface roughness extends the optical path length by scattering and reflecting across multiple internal angles within the solar spectrum of 300-1200 nm[18,19].

3.3. Morphological and Cross-Sectional Thickness (FESEM & EDAX)

The surface morphology and coating thickness were characterized using FESEM. The FESEM surface images show that whereas the monocrystalline silicon cells have the usual lattice structure, the use of RF sputtering leads to different layer packing structures as illustrated in **Figure 4(a)**. The ZnS and MoS_2 coatings showed uniform coverage of the substrate[20], whereas the composite ZnS/MoS_2 coating had a denser layer packing structure (**Figure 4(b)**). Such dense packing provides an effective optical coupling layer to ensure effective light absorption. This uniform and continuous layer reduces the chances of moisture nucleation, leading to enhanced environmental stability and increased solar cell efficiency.

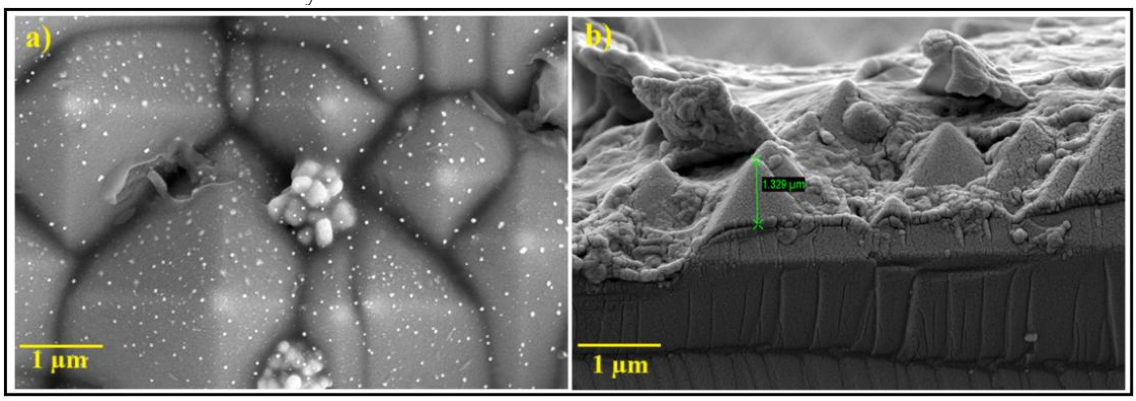


Figure 4. FESEM images of the ZnS/MoS_2 composite coating showing: (a) surface morphology and (b) cross-sectional thickness on the monocrystalline silicon substrate

The surface morphology and cross-sectional thickness of the deposited coatings were examined using FESEM. The ZnS- and MoS_2-coated samples exhibited continuous surface coverage, whereas the ZnS/MoS_2 composite coating demonstrated a denser and more uniform morphology. This compact structure provides effective coverage of the silicon surface and facilitates improved optical interaction at the coating-silicon interface. The cross-sectional FESEM images showed coating thicknesses of approximately 1.119 µm for ZnS, 1.217 µm for MoS_2, and 1.329 µm for the ZnS/MoS_2 composite coating. The greater thickness of the composite coating is associated with the combined deposition of ZnS and MoS_2 from the blended sputtering target. The uniform and continuous composite layer contributes to improved light trapping and reduced surface reflection[21].

In addition to the morphological study, an EDAX analysis was performed in parallel to confirm the elemental composition of the sputtered layer. As displayed in **Figure 5**, distinct peaks corresponding to zinc (Zn), molybdenum (Mo), and sulphur (S) are observed. Peaks corresponding to silicon (Si) were also detected, originating from the underlying silicon solar cell substrate. No other peaks were detected, indicating the purity of the deposited layer and the absence of impurities following the removal of contaminants prior to sputtering.

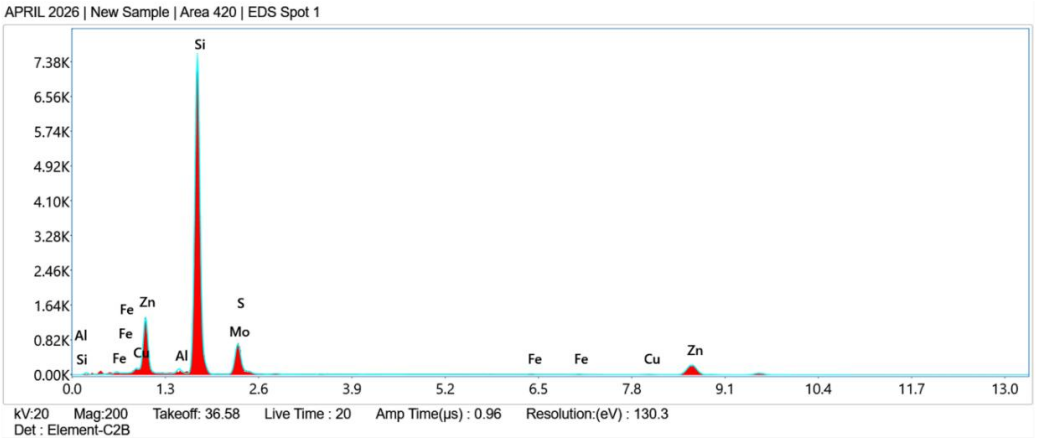


Figure 5. EDAX elemental spectrum of the sputtered layer confirming the presence of Zn, Mo, S, and the Si base material

3.4. Optical Analysis: Reflectance and Transmittance

The optical reflectance of the uncoated and coated transparent glass substrates was measured using a UV-Vis-NIR spectrophotometer over the wavelength range of 300-1200 nm to evaluate the effect of the anti-reflection coatings. The uncoated glass substrate showed a minimum reflectance of 21.95% at approximately 700 nm. As shown in **Figure 6**, the minimum reflectance decreased to 15.78% at approximately 400 nm for the ZnS-coated glass, 12.03% at approximately 800 nm for the MoS_2-coated glass, and 5.56% at approximately 470 nm for the ZnS/MoS_2 composite-coated glass. These values correspond to the minimum points observed in the reflectance spectra and do not represent the average reflectance over the entire wavelength range.

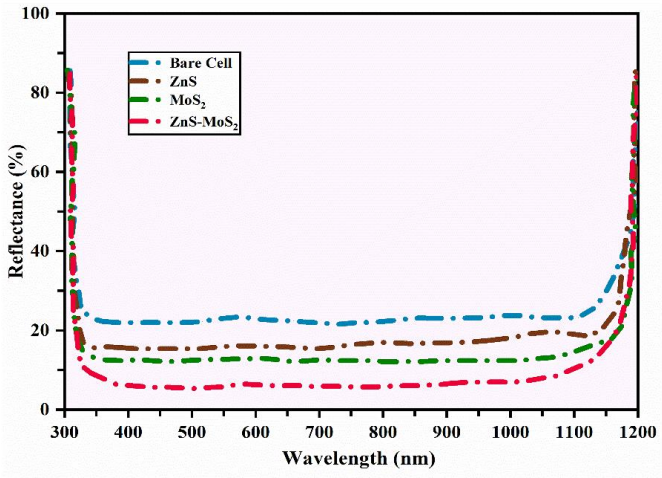


Figure 6. Optical reflectance spectra of bare and coated transparent glass substrates in the wavelength range of 300-1200 nm

The optical transmittance of the coated samples was evaluated using transparent glass substrates prepared under the same sputtering conditions as those used for the silicon solar cells. The transmittance spectra were recorded using a UV-Vis-NIR spectrophotometer over the wavelength range of 300-1200 nm. The uncoated glass substrate showed a transmittance of 77.22%, while the ZnS and MoS_2 coated glass samples exhibited higher transmittance values of 83.34% and 87.51%, respectively. As shown in **Figure 7**, the ZnS/MoS_2 composite-coated glass sample achieved the highest transmittance of 94.15%. This improvement is attributed to reduced surface reflection and enhanced light transmission through the coating. Although the transmittance measurements were performed on coated glass substrates, the corresponding reduction in reflectance on the coated

silicon solar cells allows more incident photons to reach the active silicon layer, which may contribute to the increase in short-circuit current density and PCE[22]. The measured transmittance and reflectance values are summarized in **Table 1**.

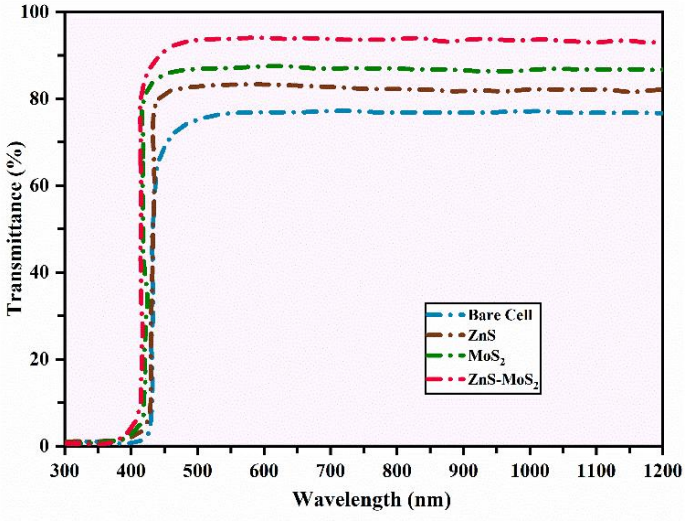


Figure 7. Optical transmittance characteristics of bare, ZnS, MoS_2, and ZnS/MoS_2 coated transparent glass substrates over the wavelength range of 300-1200 nm

Table 1. Optical transmittance and reflectance analysis of bare and coated transparent glass substrates

Specimen	Transmittance/%	Reflectance/%
Bare cell	77.22	21.95
ZnS	83.34	15.78
MoS_2	87.51	12.03
ZnS/MoS_2	94.15	5.56

The reduced reflectance of the ZnS/MoS_2 composite coating may be associated with improved optical matching between air and the silicon surface. However, the refractive index and extinction coefficient of the coating were not directly measured in this study. Therefore, the graded refractive-index effect is proposed as a possible mechanism based on the observed optical performance and should not be considered directly confirmed. Future work should include spectroscopic ellipsometry and optical modelling to verify this mechanism.

3.5. Electrical Characterization

The electrical properties of the solar cells, such as electrical resistivity (ϱ), carrier density (N), and Hall mobility (μ), were examined by the Van der Pauw method using linear four-point probes. To obtain accurate readings without damaging the ARCs, spring-loaded tungsten carbide tips were used at a fixed contact pressure of about 0.75 N. Comprehensive electrical characterization revealed that the charge transfer in the monocrystalline silicon substrate was strongly influenced by the incorporation of the ZnS/MoS_2 composite layer.

The comparative analysis showed that the bare silicon sample had the highest resistivity, which decreased after the deposition of the anti-reflection coatings. Among the coated samples, the ZnS/MoS_2 composite-coated sample exhibited the lowest resistivity and the highest measured Hall mobility and apparent carrier concentration, as shown in **Figure 8** and summarized in **Table 2**. The increase in Hall mobility may be associated with improved surface and interface quality of the sputtered coating. However, the observed carrier-concentration variation should be interpreted as an electrical response of the complete coated structure rather than a direct change in the bulk doping

concentration of silicon. The Hall-effect measurements showed differences in resistivity, Hall mobility, and apparent carrier concentration among the bare and coated samples. However, the anti-reflection coating is not expected to alter the bulk doping concentration of the silicon substrate directly. The observed variations may arise from surface and interface effects, electrical contact conditions, or measurement sensitivity in the coated structures. Therefore, these results are interpreted as comparative electrical characteristics of the complete coated samples rather than evidence of a change in the intrinsic bulk carrier concentration of silicon. The higher Hall mobility and carrier concentration observed for the ZnS/MoS_2 composite-coated cell suggest improved charge transport. This improvement may contribute to the increase in short-circuit current density and power conversion efficiency[23]. However, reduced carrier recombination was not directly confirmed because carrier-lifetime and photoluminescence measurements were not performed.

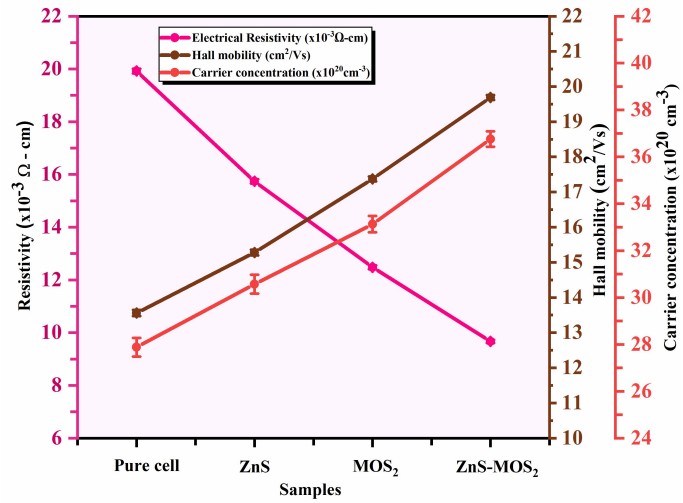


Figure 8. Comparative analysis of electrical resistivity, Hall mobility, and carrier concentration for bare and ARC-coated specimens

Table 2. Electrical results of bare cell and ARC coated solar cell specimen

Specimen	Resistivity/Ω-cm	Hall mobility/[cm^2/(V·s)]	Carrier concentration/cm^{-3}
Bare cell	19.92	13.56	27.88
ZnS	15.74	15.28	30.57
MoS_2	12.48	17.37	33.13
ZnS/MoS_2	9.67	19.69	36.76

3.6. Photovoltaic Performance and Thermal Analysis

3.6.1. Photocurrent-Voltage Characteristics

The photovoltaic performance was evaluated from I-V measurements, as shown in **Figure 9**, using a Keithley I-V source meter under natural sunlight. The current-voltage measurements were conducted under natural sunlight at an irradiation intensity of 1032 W/m^2, a cell temperature of 38 °C, and an active device area of 52 mm × 52 mm. The measurements were performed between approximately 11:00 AM and 1:00 PM under clear-sky conditions. Since the sunlight spectrum and cell temperature were not controlled according to standard AM 1.5G test conditions, the reported photovoltaic values should be considered outdoor experimental results. However, the bare and coated cells were measured under the same conditions, allowing a direct comparison of their relative performance. The performance of the cells can be gauged from the values of parameters such as VOC, JSC, and fill factor (FF).

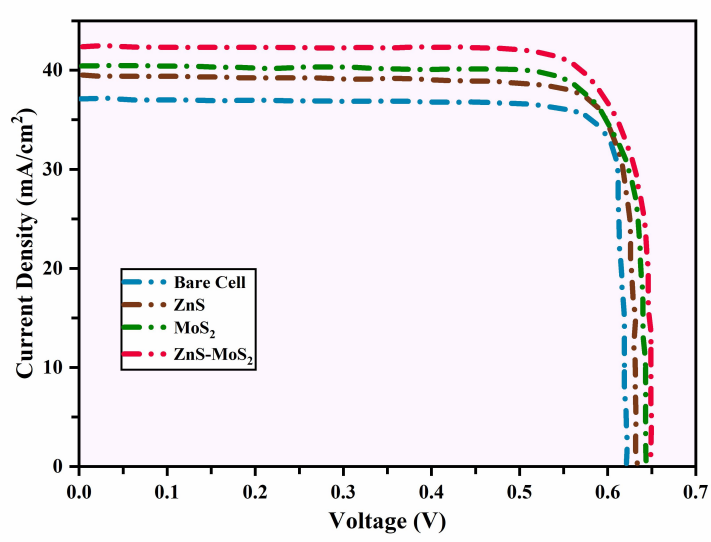


Figure 9. Photocurrent-voltage (I-V) characteristics of bare, ZnS, MoS_2, and blended ZnS/MoS_2 solar cells under sunlight exposure

The experimental investigations indicated a progressive enhancement in photovoltaic performance across the samples with the bare silicon cell exhibiting the lowest efficiency, with a VOC of 0.631 V and a JSC of 37.12 mA/cm^2 under direct sunlight. Both the ZnS- and MoS_2-coated cells outperformed the bare cell, with PCE values of 19.30% and 20.57%, respectively. However, the composite ZnS/MoS_2 layer system performed best as tabulated in **Table 3**, with a VOC of 0.648 V, a JSC of 42.37 mA/cm^2, a high FF of 80%, and a PCE of about 21.96%. This improvement can be attributed to the graded refractive-index effect, which optimizes the refractive index at the interface and minimizes Fresnel reflection losses.

Table 3. I-V measurements of bare cell, ZnS, MoS_2 and blended ZnS/MoS_2 in sunlight exposure

Sample	JSC/(mA/cm^2)	VOC/V	FF/%	PCE/%
Bare cell	37.12	0.631	74	17.33
ZnS	39.53	0.634	77	19.30
MoS_2	40.36	0.645	79	20.57
ZnS/MoS_2	42.37	0.648	80	21.96

The performance of the present ZnS/MoS_2 composite coating was compared with previously reported ZnS-, MoS_2-, and multilayer anti-reflection coatings. In the present study, the ZnS/MoS_2 composite coating reduced the reflectance of the silicon solar cell from 21.95% to 5.56% and increased the transmittance from 77.22% to 94.15%. The power conversion efficiency also increased from 17.33% for the bare cell to 21.96% for the coated cell. These results indicate that the ZnS/MoS_2 composite coating provides better light transmission and lower optical reflection than the individual ZnS and MoS_2 coatings tested under the same conditions.

The improved performance is mainly attributed to the combined optical properties of ZnS and MoS_2, the uniform composite coating, and the improved refractive-index matching between air and the silicon surface. Compared with previously reported single-layer coatings, the present composite coating provides simultaneous improvement in reflectance, transmittance, photovoltaic efficiency, and operating temperature. A quantitative comparison with related published studies is provided in **Table 4**.

Table 4. Comparison of the present ZnS/MoS_2 composite coating with previously reported anti-reflection coatings

S.No	Substrate	Coating Material	Absorbance/ %	Improvement/ %	Reflectance/ %	Improvement/ %	PCE/ %	Improvement/ %	Reference
1	Polycrystalline	SiO_2	78	6.77	19.2	17.64	14.16	14.19	[24]
2	Monocrystalline	TiO_2-Al_2O_3	93.93	29.28	8.88	62.55	19.77	29.37	[25]
3	Monocrystalline	TiO_2	-	-	8.73	75.65	14.61	27.2	[26]
4	Monocrystalline	Ta_2O_5	-	-	19.97	36.92	19.15	9.77	[27]
5	Polycrystalline	CeO_2-SiO_2	-	-	11.19	71.77	20.85	35.82	[9]

3.7. Temperature Stability Evaluation

The operating temperature of a solar cell has a significant impact on its performance, as an increase in temperature leads to higher electrical resistivity and a decrease in PCE. The thermal images in **Figure 10** show clear differences in surface temperature among the samples, with the heat distribution in bare cells being poor with a high surface temperature of about 41.2 °C.

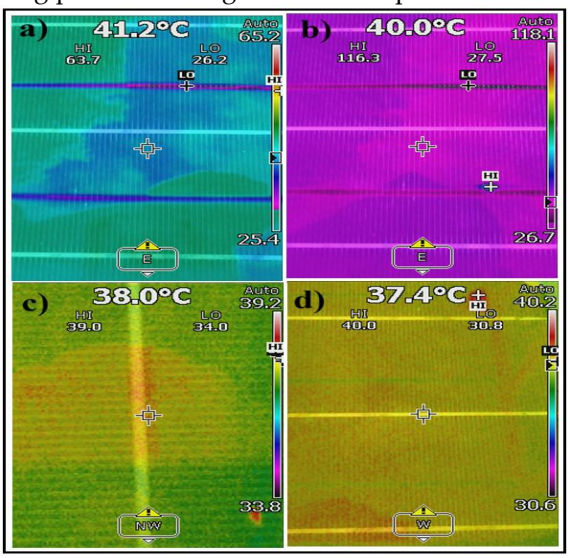


Figure 10. Surface thermal images of (a) bare cell, (b) ZnS, (c) MoS_2, and (d) ZnS/MoS_2 coated solar cells

For the ZnS and MoS_2 coatings, the surface temperature was lowered to 40 °C and 38 °C, respectively. The lowest temperature, about 33 °C, was obtained for the ZnS/MoS_2 coating. It is important to note that elevated temperatures reduce the band gap and VOC, and increase the series resistance while decreasing the shunt resistance, thereby increasing ohmic losses. Consequently, the ZnS/MoS_2 blend layer helps to minimize heat generation by maintaining a low operating temperature in the monocrystalline silicon photovoltaic cell. This result demonstrates improved short-term thermal behaviour during the measurement. However, long-term thermal stability cannot be confirmed from a single thermal-imaging test. Aging, repeated thermal-cycling, and extended outdoor exposure tests are required to evaluate long-term stability.

4. Conclusion

Indeed, the current research has successfully illustrated the design and application of efficient anti-reflection films on monocrystalline silicon solar cells through the use of RF magnetron sputtering. Among the investigated configurations, the ZnS/MoS_2 composite anti-reflection coating exhibited the most effective optically bridged interface, outperforming both the bare silicon solar cell and the individually coated ZnS and MoS_2 ARC films in terms of light management and photovoltaic efficiency. The structural analysis showed that sputtering yielded highly crystalline,

dense, and uniform thin films, with well-controlled nanometer-scale thickness. Optical analysis using UV-Vis spectroscopy revealed that the high surface reflectance of 21.95% for the bare silicon solar cell was successfully reduced to approximately 5.56% by the optimized ZnS/MoS_2 film. This significant reduction in the surface reflectance of the cells was due to a graded refractive index, which creates an optical staircase between air and the silicon substrate accompanied by destructive interference over the 300-1200 nm solar wavelength range. Consequently, the transmittance reached a peak value of 94.15%. Ultimately, these optical improvements yielded a maximum power conversion efficiency of approximately 21.96% for the ZnS/MoS_2 coated cell. These results show that TMD-based composite coatings represent a promising route toward the development of improved photovoltaic technologies. Furthermore, surface temperature measurements demonstrated that the blended ZnS/MoS_2 coating exhibited the lowest surface temperature (33 °C). The coating also showed improved short-term thermal performance under the tested conditions; however, long-term stability should be validated through accelerated aging and thermal-cycling tests. The photovoltaic performance was evaluated under natural sunlight rather than controlled AM 1.5G conditions. Therefore, future studies should validate the coating performance using a calibrated solar simulator at 1000 W/m^2, an AM 1.5G spectrum.

DECLARATIONS

About the Author

Naser A. Alsaleh is currently the head of the Industrial Engineering Department at the College of Engineering, Imam University, Riyadh, Saudi Arabia. He earned his Master's and Ph.D. degrees in Industrial Engineering from University of Minnesota-Twin Cities, Minneapolis, USA. Dr. Naser held different positions in the educational and research fields including Vice Dean for Research and Graduate Studies, Vice Dean for Quality and Development, and Head of the Research Center in the College of Engineering, Imam University, Riyadh, Saudi Arabia. Prior to that, he was the Dean of Riyadh College of Technology. Advocating, managing, and participating in research projects funded by different institutions has been prominent activities he undertook while performing his daily duties. Specifically, optimizing production operations in the industrial sector through academic research was a major concern in his practical profession. His recent research interests include improvement and optimization of manufacturing processes and the properties of its materials. Additionally, he tackled other research concerns related to optimizing the industrial production activities in the manufacturing sector, sustainable manufacturing, and industrial quality. Dr. Naser published and participated in publishing different articles covering these topics.

Author Contributions

Conceptualization: Naser A. Alsaleh
Methodology: Naser A. Alsaleh
Formal analysis: Naser A. Alsaleh
Investigation: Naser A. Alsaleh
Writing - original draft: Naser A. Alsaleh
Writing - review & editing: Naser A. Alsaleh

Acknowledgments

The author is thankful to the Deanship of Scientific Research at Imam Mohammad Ibn Saud Islamic University (IMSIU), Riyadh, Saudi Arabia for supporting this research and for BIT, India for imaging support.

Funding

This research received no external funding.

Ethics Approval and Consent to Participate
Not applicable.

Data Availability Statement
The datasets used and analyzed during the current study are available from the corresponding author on reasonable request.

Conflict of Interest
There is no conflict of interest.

AI-Generated Content Declaration
No AI tool used.

References

1. Ahmed, R.; & Tamim, M. T. R. The future of energy: Exploring renewable and non-renewable resources. *International Journal of Science Education and Science* 2025, 2(2), 85-105. https://doi.org/10.56566/ijses.v2i2.327
2. Shah, B. S.; Tailor, J. P.; Chaki, S. H.; & Deshpande, M. P. SCAPS 1D based study of hole and electron transfer layers to improve MoS_2-ZrS_2 solar cell efficiency. *Modelling and Simulation in Materials Science and Engineering* 2024, 32(6), 065015. https://doi.org/10.1088/1361-651X/ad5a2b
3. Gulomov, J., Aliev, R., Mirzaalimov, A., Mirzaalimov, N., Kakhkhorov, J., Rashidov, B., & Temirov, S. Studying the effect of light incidence angle on photoelectric parameters of solar cells by simulation. *International Journal of Renewable Energy Development* 2021, 10(4), 731-736. https://doi.org/10.14710/ijred.2021.36277
4. Parasuraman, R., & Rathnakannan, K. Thermal analysis in 3-D simulation of thin-film ZnO/MoS_2/Si solar cells. *Multiscale and Multidisciplinary Modeling, Experiments and Design* 2024, 7(4), 3815-3826. https://doi.org/10.1007/s41939-024-00440-4
5. Wang, Y., & He, J. Recent progress in outermost surface engineering for solar panels. *Nanoscale* 2025, 17(27), 16071-16099. https://doi.org/10.1039/D5NR00621J
6. Datta, R., Munson, C. D., Niemack, M. D., McMahon, J. J., Britton, J., Wollack, E. J., Beall, J., Devlin, M. J., Fowler, J., Gallardo, P., Hubmayr, J., Irwin, K., Newburgh, L., Nibarger, J. P., Page, L., Quijada, M. A., Schmitt, B. L., Staggs, S. T., Thornton, R., & Zhang, L. Large-aperture wide-bandwidth antireflection-coated silicon lenses for millimeter wavelengths. *Applied Optics* 2013, 52(36), 8747-8758. https://doi.org/10.1364/AO.52.008747
7. Uzum, A., Kanda, H., Fukui, H., Izumi, T., Harada, T., & Ito, S. Totally vacuum-free processed crystalline silicon solar cells over 17.5% conversion efficiency. *Photonics* 2017, 4(3), 42. https://doi.org/10.3390/photonics4030042
8. Chen, D. Anti-reflection (AR) coatings made by sol-gel processes: A review. *Solar Energy Materials and Solar Cells* 2001, 68(3-4), 313-336. https://doi.org/10.1016/S0927-0248(00)00365-2
9. Kanmaz, I., Tomakin, M., & Uzum, A. Analysis of CeO_2/SiO_2 double-layer thin film stack with antireflection effect for silicon solar cells. *Journal of Materials Science: Materials in Electronics* 2024, 35(22), 1497. https://doi.org/10.1007/s10854-024-13245-5
10. Lien, S. Y., Wuu, D. S., Yeh, W. C., & Liu, J. C. Tri-layer antireflection coatings (SiO_2/SiO_2-TiO_2/TiO_2) for silicon solar cells using a sol-gel technique. *Solar Energy Materials and Solar Cells* 2006, 90(16), 2710-2719. https://doi.org/10.1016/j.solmat.2006.04.001
11. Hou, G., García, I., & Rey-Stolle, I. High-low refractive index stacks for broadband antireflection coatings for multijunction solar cells. *Solar Energy* 2021, 217, 29-39. https://doi.org/10.1016/j.solener.2021.01.060
12. Prashantha, S., Rajasekar, R., Gobinath, V. K., Raja, G., Subha, K., & Manjunath, K. S. Augmenting the performance of photovoltaic cell through surface coating of molybdenum disulphide. *Chalcogenide Letters* 2021, 18(4), 161-170. https://doi.org/10.15251/CL.2021.184.161
13. Xue, C. R., Gu, Y. Q., & Deng, M. L. Investigation on antireflection coatings for silicon solar cells. *Applied Mechanics and Materials* 2014, 521, 33-36. https://doi.org/10.4028/www.scientific.net/AMM.521.33

14. Karimzadeh, S., Safaei, B., Yuan, C., & Jen, T. C. Emerging atomic layer deposition for the development of high-performance lithium-ion batteries. *Electrochemical Energy Reviews* 2023, 6(1), 24. https://doi.org/10.1007/s41918-023-00192-8
15. Rooprai, R. S., Singh, V., Singh, J., Bansal, A., & Singla, A. K. Optimizing wear performance in vanadium-carbide-reinforced AISI316 composite claddings via wire arc additive manufacturing. *Journal of Materials Engineering and Performance* 2025, 34(23), 28374-28390. https://doi.org/10.1007/s11665-025-11312-4
16. Rooprai, R. S., Singh, J., Bansal, A., Singh, V., & Singla, A. K. RSM investigation of dry abrasion in WAAM fabricated inconel 625 cladding on EN8 steel. *Progress in Additive Manufacturing* 2026, 11(3), 2373-2391. https://doi.org/10.1007/s40964-025-01473-y
17. Velu Kaliyannan, G., Gunasekaran, R., Rathanasamy, R., Kandasamy, S., Anand Raj, M. K., Sivaraj, S., & Sellamuthu, K. Enhanced mechanical and tribological behavior of Al356 hybrid composites reinforced with TiB_2-SiC-fly ash for automotive applications. *Materials Testing* 2026, 68(4), 755-765. https://doi.org/10.1515/mt-2025-0424
18. Springer, J., Poruba, A., & Vanecek, M. Improved three-dimensional optical model for thin-film silicon solar cells. *Journal of Applied Physics* 2004, 96(9), 5329-5337. https://doi.org/10.1063/1.1784555
19. Yeh, P. S., Chen, C. W., Yang, B. R., & Hong, L. S. Light-scattering effectiveness of two-dimensional disordered surface textures in thin-film silicon solar cells. *Applied Optics* 2014, 53(13), 2847-2852. https://doi.org/10.1364/AO.53.002847
20. Baranowska-Korczyc, A., Kościński, M., Coy, E. L., Grześkowiak, B. F., Jasiurkowska-Delaporte, M., Peplińska, B., & Jurga, S. ZnS coating for enhanced environmental stability and improved properties of ZnO thin films. *RSC Advances* 2018, 8(43), 24411-24421. https://doi.org/10.1039/C8RA02823K
21. Narasimhan, V. K., & Cui, Y. Nanostructures for photon management in solar cells. *Nanophotonics* 2013, 2(3), 187-210. https://doi.org/10.1515/nanoph-2013-0001
22. Liang, H., Wang, F., Cheng, Z., Xu, C., Li, G., & Shuai, Y. Full-spectrum solar energy utilization and enhanced solar energy harvesting via photon anti-reflection and scattering performance using biomimetic nanophotonic structure. *ES Energy & Environment* 2020, 8, 29-41. https://doi.org/10.30919/esee8c456
23. Reddy, R. M., Chirag, S., Anu, T., Venkataramanan, A. R., Karthikeyan, S., Palaniswamy, D., Venugopal Goud, E., Dineshbabu, N., & Thirugnanasambandham, T. Boosting power efficiency in polycrystalline silicon solar cells: Antimony selenide sputter coating with advanced optical, electrical, and thermal insights. *Chalcogenide Letters* 2025, 22(7), 615-624. https://doi.org/10.15251/CL.2025.227.615
24. Anbupalani, M. S., Venkatachalam, C. D., Rathanasamy, R., & Velu Kaliyannan, G. Employing SiO_2/TiO_2/ZrO_2 blends for boosting the power conversion efficiency of polycrystalline Si solar cells. *Journal of Materials Science: Materials in Electronics* 2023, 34(33), 2184. https://doi.org/10.1007/s10854-023-11589-y
25. Alkallas, F. H., Alghamdi, S. M., Velu Kaliyannan, G., Gunasekaran, R., Rathanasamy, R., Ben Gouider Trabelsi, A., Elsharkawy, W., Mostafa, A. M., & Palaniappan, S. K. Enhanced efficiency of mono-crystalline Si solar cells utilizing RF sputtered TiO_2-Al_2O_3 blended anti-reflection coating for optimal sunlight transmission and energy conversion. *Ceramics International* 2024, 50(9), 14865-14877. https://doi.org/10.1016/j.ceramint.2024.01.402
26. Hocine, D., Belkaid, M. S., Pasquinelli, M., Escoubas, L., Simon, J. J., Rivière, G. A., & Moussi, A. Improved efficiency of multicrystalline silicon solar cells by TiO_2 antireflection coatings derived by APCVD process. *Materials Science in Semiconductor Processing* 2013, 16(1), 113-117. https://doi.org/10.1016/j.mssp.2012.06.004
27. Sagar, R., & Rao, A. Nanoscale TiO_2 and Ta_2O_5 as efficient antireflection coatings on commercial monocrystalline silicon solar cell. *Journal of Alloys and Compounds* 2021, 862, 158464. https://doi.org/10.1016/j.jallcom.2020.158464



© 2026 by the authors. Submitted for possible open access publication under the terms and conditions of the Creative Commons Attribution (CC BY) license (http://creativecommons.org/licenses/by/4.0/).